ADVANCES IN ATMOSPHERIC SCIENCES, VOL. 40, JANUARY 2023, 177–185

• **Notes & Letters** •

Understanding the Development of the 2018/19 Central Pacific El Niño

Chengyang GUAN[1], Xin WANG[*2,3,4], and Haijun YANG[5]

[1]*College of Ocean Science and Engineering*, *Shandong University of Science and Technology*, *Qingdao* 266590, *China*

[2]*State Key Laboratory of Tropical Oceanography*, *South China Sea Institute of Oceanology*, *Chinese Academy of Sciences*, *Guangzhou* 510301, *China*

[3]*Southern Marine Science and Engineering Guangdong Laboratory (Guangzhou)*, *Guangzhou* 511458, *China*

[4]*Innovation Academy of South China Sea Ecology and Environmental Engineering*, *Chinese Academy of Sciences*, *Guangzhou* 510301, *China*

[5]*Department of Atmospheric and Oceanic Sciences*, *Fudan University*, *Shanghai* 200438, *China*

(Received 4 November 2021; revised 17 May 2022; accepted 18 May 2022)

ABSTRACT

A central Pacific (CP) El Niño event occurred in 2018/19. Previous studies have shown that different mechanisms are responsible for different subtypes of CP El Niño events (CP-I El Niño and CP-II El Niño). By comparing the evolutions of surface winds, ocean temperatures, and heat budgets of the CP-I El Niño, CP-II El Niño, and 2018/19 El Niño, it is illustrated that the subtropical westerly anomalies in the North Pacific, which led to anomalous convergence of Ekman flow and surface warming in the central equatorial Pacific, played an important role in the 2018/19 El Niño event as well as in the CP-II El Niño. Although the off-equatorial forcing played a vital role, it is found that the equatorial forcing acted as a driving (damping) term in boreal spring (summer) of the 2018/19 El Niño. The 2018/19 El Niño provides a timely and vivid example that helps illustrate the proposed mechanism of the CP El Niño, which could be leveraged to improve El Niño predictability.

Key words: El Niño, subtropical Pacific, westerly anomalies, Ekman transport

Citation: Guan, C. Y., X. Wang, and H. J. Yang, 2023: Understanding the development of the 2018/19 central Pacific El Niño. *Adv. Atmos. Sci.*, **40**(1), 177−185, https://doi.org/10.1007/s00376-022-1410-1.

Article Highlights:

- The 2018/19 El Niño was a CP El Niño, and the warm SST anomalies originated in the subtropical North Pacific.
- Ekman transport caused by the westerly anomalies in the northern subtropical Pacific was vital for the 2018/19 El Niño as well as the CP-II El Niño proposed in a previous study.
- Different from the composite CP-II El Niño, equatorial air–sea coupling processes could have contributed to the development of the 2018/19 El Niño in spring.

1. Introduction

El Niño Southern Oscillation (ENSO) is the dominant interannual variation of sea surface temperature (SST) in the tropical Pacific region. The event-to-event diversity of individual ENSO events can lead to different climate impacts (Ashok et al., 2007; Wang and Wang, 2013, 2014; Capotondi et al., 2015; Yu et al., 2017). El Niño events are often classified as Eastern Pacific (EP) or Central Pacific (CP) El Niño events (Yu and Kao, 2007; Kao and Yu, 2009; Yu and Kim, 2011). An EP El Niño first exhibits surface warming in the cold-tongue region in the eastern Pacific, while a CP El Niño first exhibits surface warming in the central tropical Pacific. The latter is also referred to as an El Niño Modoki (Ashok et al., 2007) or a dateline El Niño (Larkin and Harrison, 2005).

Recent studies have revealed that different types of El Niño events are dominated by different physical processes (Kug et al., 2009; Yu et al., 2010; Chen et al., 2015; Lai et al., 2015; Wang et al., 2019b). Kug et al. (2009) demonstrated that a CP El Niño arises mainly from zonal advective feedback, while warming in the eastern tropical Pacific is suppressed by enhanced upwelling and evaporation caused by equatorial easterly anomalies. Yu et al. (2010) pointed out that during the development of a CP El Niño, SST anomalies first appear in the northeastern subtropical Pacific and

* Corresponding author: Xin WANG
Email: wangxin@scsio.ac.cn

extrend towards the central equatorial Pacific through wind–evaporation–SST (WES) feedback (Xie and Philander, 1994). There are also studies suggesting that the forcings from the northern subtropical Pacific could trigger the development of a CP El Niño via the seasonal footprinting mechanism (Vimont et al., 2001; Yeh et al., 2015; Yu and Fang, 2018; Fang and Yu, 2020). Chen et al. (2015) and Lai et al. (2015) emphasized that the diversity of El Niño events is a combined effect of both zonal wind anomalies and subsurface temperature anomalies in the equatorial Pacific.

Wang and Wang (2013) investigated the diversity in SST evolution and climate impact of CP El Niño events and further classified them into two subtypes, Modoki-I and Modoki-II (referred to as CP-I and CP-II hereafter). Despite the similarity of both CP types warming in the central tropical Pacific, they have distinctly different spatial patterns and regional climatic effects (Liu et al., 2014; Wang and Wang, 2014; Tan et al., 2016; Liu et al., 2017; Chen et al., 2019; Wang et al., 2020b; Kim et al., 2021). A CP-I (CP-II) El Niño tends to induce positive (negative) SST anomalies in the South China Sea during developing autumn, mainly by affecting the latent heat flux (Tan et al., 2016). Associated with a weaker Walker circulation in the Indo–Pacific region, a CP-I (CP-II) El Niño favors a positive (negative) Indian Ocean Dipole via the Bjerknes feedback (Wang and Wang, 2014). As for the western Pacific subtropical high during the decaying summer, a CP-I (CP-II) El Niño imposes little (strong positive) impact (Chen et al., 2019, 2021a). Wang et al. (2018) came up with an index to identify the two subtypes of CP El Niño events and showed that CP-II events occurred the most often after 1990. Wang et al. (2019c) investigated CP El Niño events occurring from 1900 to 2010 by analyzing the heat budget of the mixed layer water in the Niño-4 region (5°S–5°N, 160°E–150°W) and discovered that zonal advective (Ekman pumping) feedback is the leading contributor to CP-I (CP-II) El Niño events. Chen (2021b) concluded that a CP-I El Niño is triggered by the weakening of the Australian winter monsoon, while a CP-II El Niño is mainly forced by the Pacific Meridional Mode (PMM) via WES feedback.

In 2018/19, an El Niño event occurred, with the warming center located at the Date Line. The SST anomalies first appeared in the northern subtropical Pacific and then extended towards the central tropical Pacific. The surface warming was stronger in the Niño-4 region (5°S–5°N, 160°E–150°W) than in the Niño-3 region (5°S–5°N, 150°–90°W; Fig. 1). Based on observations and model forecasts, Liu et al. (2020) argued that the central tropical Pacific warming in the 2018/19 El Niño, along with tropical Atlantic warming and interdecadal variation, is one of the major factors leading to the extremely wet winter of 2018/19 in the lower reach of the Yangtze River. Wang et al. (2020a) suggested that the 2018/19 El Niño induced a remote teleconnection pattern with pronounced low-level southerly anomalies over East China, which transported moisture from oceans to the continent and caused persistent rainy days in the 2018/19 winter in Shanghai, China.

The 2018/19 El Niño event presents an opportunity to examine the genesis mechanisms of a CP El Niño. In this work, the physical processes associated with the 2018/19 El Niño are analyzed. It is demonstrated that the off-equatorial forcings in the northern subtropical Pacific are the primary cause of the 2018/19 El Niño. The contributions of the equatorial forcings, however, can be opposing during different stages.

2. Data and method

Monthly SSTs from the Extended Reconstructed Sea Surface Temperature, version 5 (ERSST v5) dataset with a

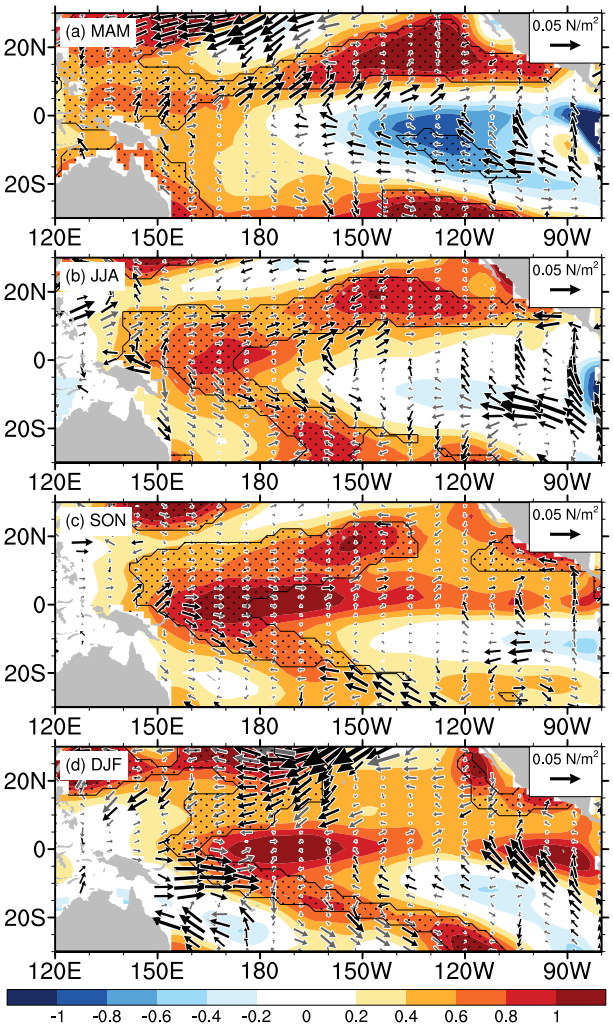

Fig. 1. Evolution of SST (shading, °C) and wind stress (vector, N m^{-2}) anomalies in the tropical Pacific during the development of the 2018/19 El Niño. (a) MAM, (b) JJA, and (c) SON indicate the periods of March–April–May, June–July–August, and September–October–November in 2018, respectively. (d) DJF indicates the period from December 2018 to February 2019. Black vectors indicate wind stress anomalies exceeding ±1.5 standard deviations. The dotted area indicates where SST anomalies exceed ±1.5 standard deviations.

resolution of 2.0° × 2.0° (Huang et al., 2017), monthly sea level pressures, surface winds and heat fluxes from the National Centers for Environmental Prediction-National Center for Atmospheric Research (NCEP/NCAR) Reanalysis 1 with a resolution of 2.5° × 2.5° (Kalnay et al., 1996), and monthly wind stress, ocean current, and temperature data from the Global Ocean Data Assimilation System (GODAS) (Behringer and Xue, 2004) with a horizontal resolution of 0.333° latitude × 1.0° longitude are used to analyze the evolution of the 2018/19 El Niño. Ocean current and temperature data at 40 vertical levels from GODAS are used. These monthly variables cover the period from 1950 to January 2019. Monthly oceanic current and temperature data from the Simple Ocean Data Assimilation (SODA) 2.2.4 (Carton and Giese, 2008; Giese and Ray, 2011) and monthly sea surface wind data from the Twentieth Century Global Reanalysis Version 2 (20CR v2) (Compo et al., 2011), with a longer time span covering 1900–2010, are used for the composite analyses of CP-I and CP-II El Niño events. The 20CR v2 data are on a global T62 Gaussian grid. Pentad wind stress data from GODAS are also analyzed for the development of the 2018/19 El Niño. The precipitation rate data is from the Global Precipitation Climatology Centre (GPCC) Monitoring Product Version 6 (2014–present; Schneider et al., 2011) and Version 7 (1901–2013; Schneider et al., 2016), with a resolution of 1.0° × 1.0°.

The classification of EP or CP El Niño is based on the El Niño Modoki index (EMI) proposed by Ashok et al. (2007):

$$\mathrm{EMI} = [\mathrm{SSTA}]_{\mathrm{C}} - 0.5[\mathrm{SSTA}]_{\mathrm{W}} - 0.5[\mathrm{SSTA}]_{\mathrm{E}}\,, \qquad (1)$$

where the subscripts C, W, and E indicate the SST anomalies averaged in the central (165°E–140°W, 10°S–10°N), western (125°–145°E, 10°S–20°N), and eastern (110°–70°W, 15°S–5°N) Pacific, respectively. The El Niño event is considered a "typical" CP event when the EMI is equal to or greater than 0.7σ, where σ is the climatological standard deviation.

CP El Niño events, as mentioned above, can be further classified as CP-I or CP-II El Niño events, with reference to their opposite influences on the precipitation in southern China (Wang and Wang, 2013). Additionally, Wang et al. (2018) developed a new index (CP-II index in this paper) to identify the subtypes of CP El Niño events. The CP-II index is defined as the leading principal component of multivariate empirical orthogonal function analysis of the normalized EMI, Niño-4 index, and 850-hPa relative vorticity anomalies averaged near the Philippine Sea (115°–145°E, 10°–25°N) during boreal autumn. CP El Niño events with a CP-II index larger than one standard deviation are designated as a CP-II El Niño.

Following Wang and Wang (2013), seven CP-I El Niño events (1914/15, 1940/41, 1941/42, 1963/64, 1987/88, 1990/91, and 2002/03) and six CP-II El Niño events (1968/69, 1979/80, 1991/92, 1992/93, 2004/05, and 2009/10) are selected as the historical collections. Monthly data are utilized to conduct the heat budget analysis of the ocean mixed-layer temperature based on the equation from Huang et al. (2010):

$$T_{\mathrm{t}}' = Q_u' + Q_v' + Q_w' + Q_q' + R\,, \qquad (2)$$

where the primes indicate temporal anomalies. T_{t} represents the temperature tendency. Q_u, Q_v, and Q_w represent the zonal, meridional, and vertical advective feedback. Q_q represents the net surface flux. R represents the residuals. The ocean mixed-layer depths, defined as the depth where the buoyancy difference with respect to the surface level is equal to 0.03 cm s^{-2}, are from the GODAS dataset.

The advection terms on the right side of Eq. (2) are further decomposed as

$$Q_u' = -\overline{u}\frac{\partial T'}{\partial x} - u'\frac{\partial \overline{T}}{\partial x} - u'\frac{\partial T'}{\partial x} + \overline{u'\frac{\partial T'}{\partial x}}\,, \qquad (3)$$

$$Q_v' = -\overline{v}\frac{\partial T'}{\partial y} - v'\frac{\partial \overline{T}}{\partial y} - v'\frac{\partial T'}{\partial y} + \overline{v'\frac{\partial T'}{\partial y}}\,, \qquad (4)$$

$$Q_w' = -\overline{w}\frac{\partial T'}{\partial z} - w'\frac{\partial \overline{T}}{\partial z} - w'\frac{\partial T'}{\partial z} + \overline{w'\frac{\partial T'}{\partial z}}\,, \qquad (5)$$

$$Q_q' = \frac{Q_{\mathrm{net}}'}{\rho c_p h}\,, \qquad (6)$$

where T is the ocean mixed-layer temperature. u, v, and w represent the zonal, meridional, and vertical current, respectively. ρ is the seawater density. c_p is the specific heat capacity of seawater under constant pressure. h is the depth of the mixed layer. The overbars indicate temporal average.

3. Results

3.1. *Classification of the 2018/19 El Niño*

Firstly, the EMI in 2018 is calculated, which exceeds 0.7σ from June to November [Fig. S1 in the electronic supplementary material (ESM)]. Thus, the 2018/19 El Niño is identified as a CP El Niño. Secondly, there are two ways to separate CP-I and CP-II El Niño events. The southern China rainfall during the boreal autumn of 2018 was significantly positive, the same as that of a CP-I El Niño (Fig. S2 in the ESM). The CP-II index of 2018 is 0.87σ (less than one standard deviation). So, the 2018/19 El Niño should be categorized as a CP-I El Niño event under either classification approach. The 2018/19 El Niño exhibited equatorial westerly anomalies during the developing February and March (Fig. 2c). The equatorial westerly anomalies generated downwelling Kelvin waves that propagated eastward and caused positive zonal advective feedback (Fig. 3b), leading to positive ocean heat content (OHC) anomalies in the central Pacific during the developing February to March (Fig. 2c). All of these

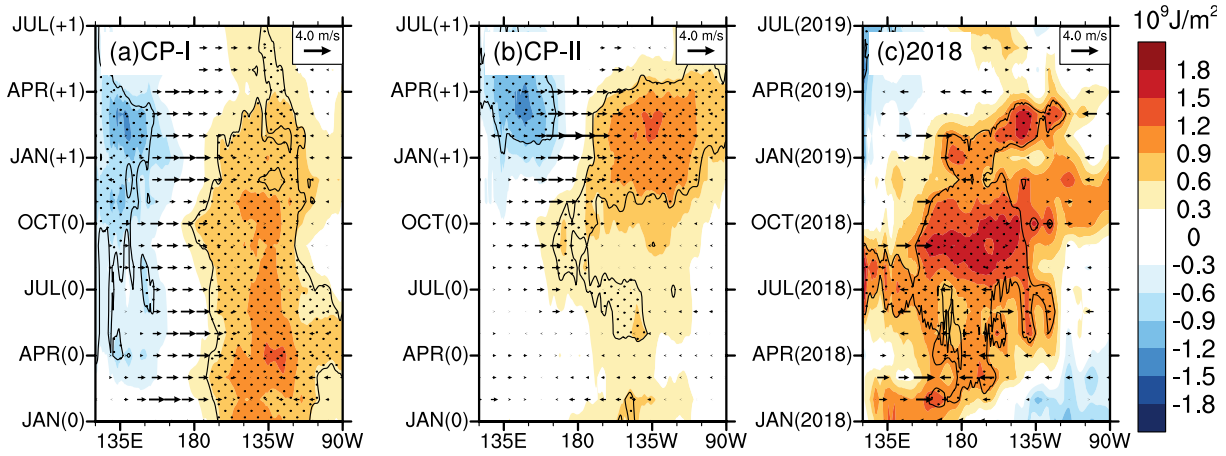

Fig. 2. Evolutions of ocean heat content (OHC) anomalies in the top 300 m (shading; units: 10^9 J m^{-2}) and surface zonal wind anomalies (vector; units: m s^{-1}) in the equatorial Pacific (averaged between 5°S–5°N) during the (a) CP-I El Niño, (b) CP-II El Niño, and (c) 2018/19 El Niño. In (a) and (b), (0) and (+1) on the *y*-axis indicate the developing and decaying year, respectively. Black dots in (a) and (b) denote areas exceeding the 90% confidence level. Black dots in (c) denote areas exceeding ±1 standard deviation.

features are the precursors of a CP-I El Niño, and the zonal advective feedback is supposed to support the warming in the central equatorial Pacific until the peak. The subsequent development process, however, tells a different story.

3.2. *Developing processes*

Easterly anomalies spread across the equatorial Pacific in late boreal spring and summer (April to August), induced negative zonal advective feedback (Fig. 3b), and suppressed the increase of oceanic subsurface temperature in the central equatorial Pacific. Yet, the oceanic subsurface temperature in the central equatorial Pacific still increased notably in late boreal summer without significant westerly anomalies in the western equatorial Pacific (Figs. 2b, c). It will be demonstrated below that this notable warming in the central equatorial Pacific is mainly ascribed to the Ekman feedback induced by the subtropical westerly anomalies.

During the spring of 2018, westerly anomalies were mainly located in the central subtropical Pacific (5°–10°N, 170°E–130°W), and positive SST anomalies (exceeding 1°C) were in the northeastern subtropical Pacific (Fig. 1a). Under the influence of WES feedback, the surface warming extended from the northeastern Pacific to the central equatorial Pacific. When the central Pacific SST anomalies were adequately positive, westerly anomalies arose in the western equatorial Pacific (Fig. 1c). The westerly anomalies and the surface warming in the central Pacific enhanced themselves through Bjerknes feedback (Bjerknes, 1969) and peaked in the boreal winter of 2018/19. Particularly, the developing patterns of SST anomalies and wind anomalies resembled those of a CP-II El Niño (Figs. S3e–h in the ESM).

Evolutions of composite OHC anomalies in the top 300 m and surface zonal wind anomalies in the equatorial Pacific during CP-I and CP-II El Niño events are illustrated in Fig. 2a and Fig. 2b, respectively. For the CP-I El Niño events, the significantly positive OHC anomalies in the eastern-central Pacific and westerly anomalies in the western-central equatorial Pacific persist during the whole developing year, indicating that the equatorial ocean and the atmosphere are well coupled. For the CP-II El Niño events, OHC anomalies in the central equatorial Pacific begin to increase remarkably in developing summer, even though strong westerly anomalies have not taken place in the equatorial Pacific yet. According to Wang et al. (2019c), the warming in the central Pacific is mainly caused by the westerly anomalies in the northern subtropical Pacific via Ekman feedback. As a critical feature of a CP-II El Niño, this process recurred in 2018. During the summer (June–August) of 2018, while strong westerly anomalies were still absent in the western-central equatorial Pacific, the OHC anomalies increased sharply (Fig. 2c). After the increase of OHC in the central equatorial Pacific, westerly anomalies prevailed in the western equatorial Pacific until the spring of 2019 (Fig. 2c).

Characteristic features of the CP-I, CP-II, and 2018/19 El Niño mentioned above include the evolutions of equatorial SST anomalies (Fig. S4 in the ESM) and thermocline anomalies (Fig. S5 in the ESM). In particular, the multi-occurrence of downwelling Kelvin waves, which is attributed to the evolution characteristics of the wind anomalies, during the boreal spring, autumn, and winter of 2018 is clearly illustrated in Fig. S1c and Fig. S4c.

3.3. *Mixed-layer heat budget analysis*

To isolate the warming mechanism, the ocean mixed-layer heat budget for the Niño-4 region is analyzed for the CP-I, CP-II, and 2018/19 El Niño. For the CP-I El Niño, the leading contributors to the mixed-layer temperature warming are the zonal and meridional advective feedbacks (Fig. S6a in the ESM). During the whole developing phase of the CP-I El Niño, the contribution from vertical advective feedback remains small. In comparison, vertical advective feedback is the leading accumulative contributor in boreal spring and sum-

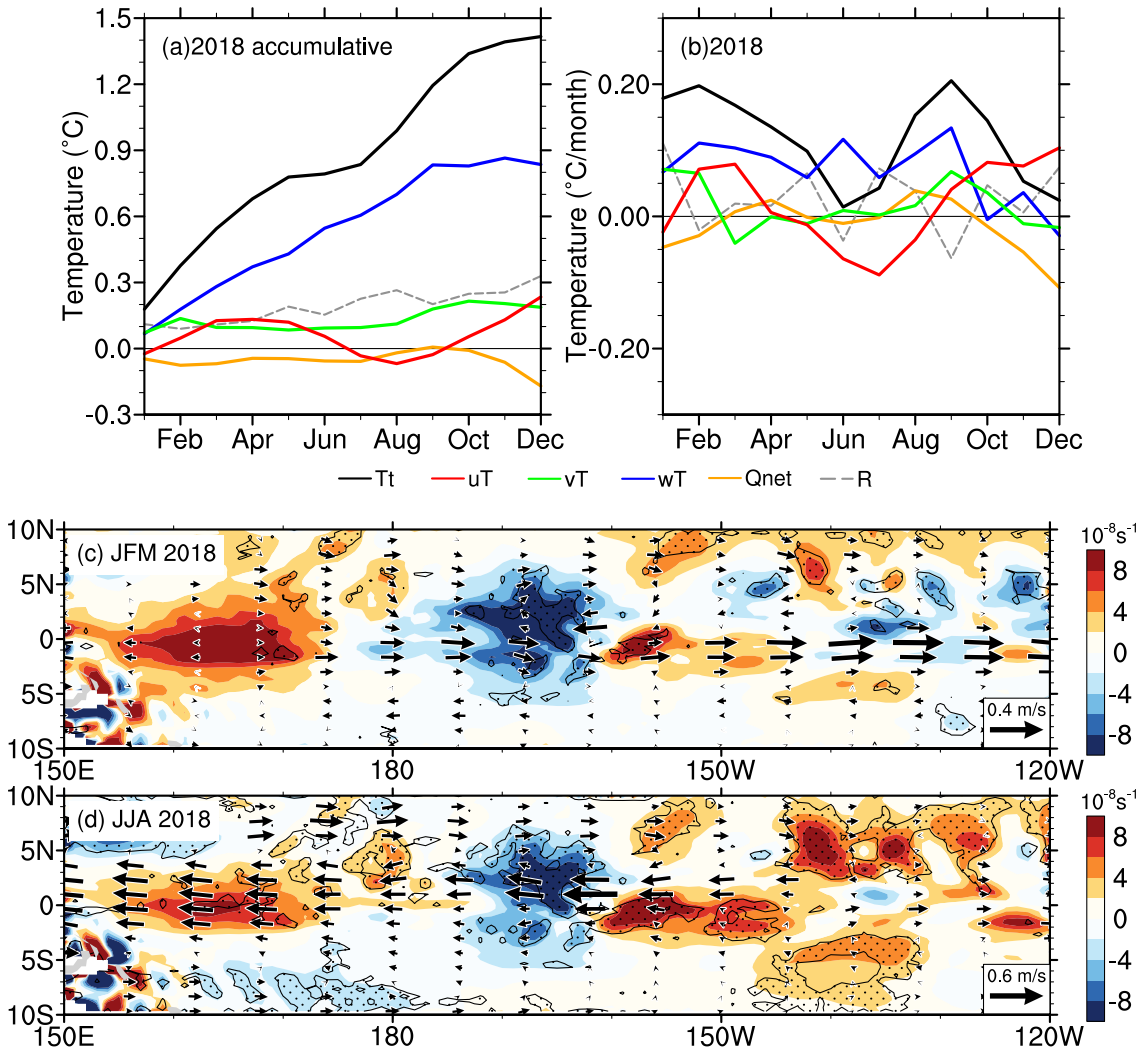

Fig. 3. (a) Ocean mixed-layer heat budget analysis of the Niño-4 region during 2018 and (b) accumulative contributions of each term. Anomalies of horizontal current (vector) in the upper 150 m and its divergence (shading) in (c) January–February–March (JFM) and (d) June–July–August (JJA) 2018. In (a) and (b), T_t represents the temperature trend anomaly. uT, vT and wT represent anomalies of zonal, meridional and vertical advection, respectively. Qnet represents the anomaly of the net surface heat flux. *R* represents the residuals. Black dots in (c) and (d) denote areas exceeding ±1.5 standard deviations.

mer during the CP-II El Niño (Fig. S6c). Due to the absence of significant surface zonal wind anomalies in the western equatorial Pacific (Fig. 2b), the contributions of zonal advective feedback and meridional advective feedback are rather weak in boreal spring (Fig. S6d).

It is evident that vertical advective feedback plays the leading role in the development of the 2018/19 El Niño, especially in boreal spring and autumn (Figs. 3a, b). Thus, the positive ocean temperature anomalies in the central equatorial Pacific during the CP-II and 2018/19 El Niño can reach a deeper depth than those during the CP-I El Niño (Fig. S7 in the ESM). The only characteristic in line with the CP-I El Niño is the early boost of the zonal advective feedback. The contribution from zonal advective feedback reached its peak before April of 2018 (Fig. 3b), when westerly anomalies prevailed in the western equatorial Pacific and generated downwelling Kelvin waves that propagated eastward to the central Pacific (Fig. 2c). Associated with eastward current anomalies in the upper equatorial Pacific (Fig. 3c), the resultant positive zonal advective feedback made a considerable contribution to the warming of the central Pacific. Thus, the upper-ocean temperature warms much earlier in the 2018/19 El Niño than it does in the CP-II El Niño (Fig. S7i), consistent with the results of the OHC evolution (Fig. 2c). In July, easterly anomalies took the place of the westerly anomalies in the western Pacific (Fig. 2c), generating upwelling Kelvin waves, and the equatorial current anomalies turned to be westward (Fig. 3d). Thus, the zonal advective feedback reversed to be negative, and the Niño-4 temperature trend anomaly dropped sharply. While the zonal current anomalies changed their direction, the central equatorial Pacific (Niño-4 region) maintained anomalous convergence in the upper ocean the entire time (Figs. 3c, d). In this way, the climatological upwelling in the central equatorial Pacific was hindered,

and the Ekman feedback kept the Niño-4 temperature anomalies increasing.

The upper-layer divergence in the central equatorial Pacific during 2018 summer is further decomposed into two parts (Fig. 4). One part is led by the zonal current anomalies, and the other is led by the meridional current anomalies. While the zonal-led divergence anomalies ($\mathrm{d}u'/\mathrm{d}x$) are mainly positive in the Niño-4 region (averaged 1.87×10^{-8} s^{-1}; Fig. 4b), the meridional-led divergence anomalies ($\mathrm{d}v'/\mathrm{d}y$) are mostly negative (averaged -2.31×10^{-8} s^{-1}; Fig. 4d). Therefore, the total divergence in the Niño-4 region adds up to be negative (i.e., an anomalous convergence) and is dominated by the meridional-led part.

3.4. *Influence of the subtropical westerly wind forcing*

In order to understand the influence of subtropical westerly wind forcing on the anomalous convergence through Ekman transport, the meridional Ekman flow is calculated by:

$$V_{\mathrm{E}} = \frac{\tau_x}{\rho f}, \tag{7}$$

where V_{E} is the meridional Ekman current (positive for northward flow, negative for southward flow), τ_x is the zonal wind stress, ρ is the seawater density (1025 kg m^{-3}), and f is the Coriolis parameter ($f = 2\Omega\sin\theta$, with Ω and θ equal to Earth's angular velocity and latitude, respectively). Zonal wind stress averaged within (6°–10°N, 160°E–150°W) is used to represent the westerly wind forcing in the subtropical North Pacific. The resultant V_{E} anomaly in 2018 summer is –0.94 m s^{-1} (see Fig. S8 in the ESM for details), while the anomaly of the mean meridional current in the mixed layer across the section (5°N, 160°E–150°W) is –0.32 m s^{-1}. This demonstrates the vital role of the subtropical westerly wind forcing on the central equatorial Pacific.

To sum up, the anomalous convergence in the central equatorial Pacific was induced by the off-equatorial westerly anomalies (Figs. 1a, b). It favored the warming in the central

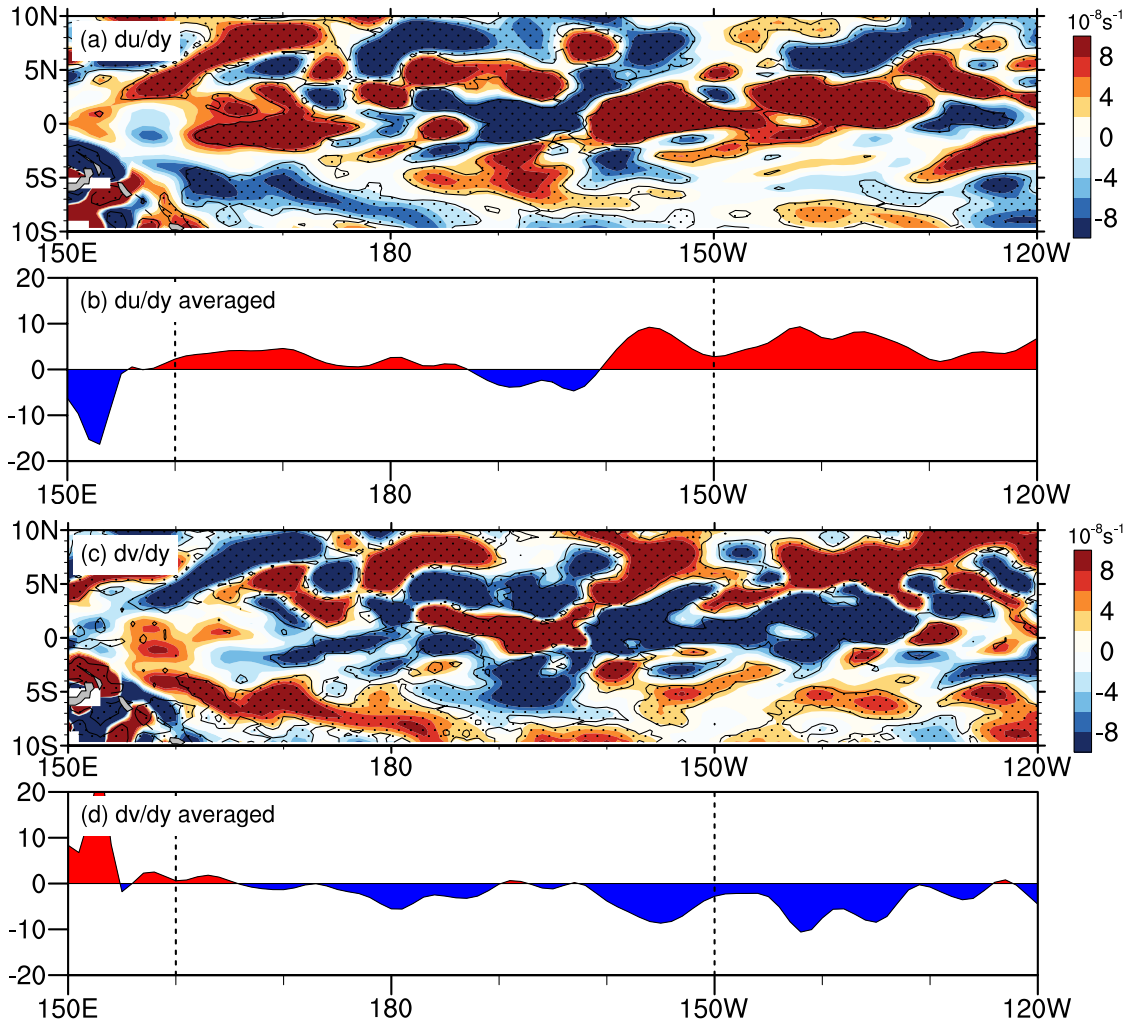

Fig. 4. (a) The oceanic convergence in the upper 150 m solely led by the zonal current anomalies ($\mathrm{d}u'/\mathrm{d}x$) in June–July–August (JJA) 2018. (b) The oceanic convergence in (a) averaged between 5°S and 5°N (units: 10^{-8} s^{-1}). (c) and (d) are the same as (a) and (b), except that the convergence is solely led by the meridional current anomalies ($\mathrm{d}v'/\mathrm{d}y$). Dashed lines in (b) and (d) indicate the zonal boundaries of the Niño-4 region.

equatorial Pacific by suppressing the climatological upwelling and inducing positive vertical advective feedback (Wang et al., 2019c). When the Niño-4 region got warm enough in autumn, the Bjerknes feedback became effective, bringing about westerly anomalies and downwelling Kelvin waves again in the equatorial Pacific. As a result, the zonal advective feedback became positive and dominant. In the wake of the propagation of downwelling Kelvin waves, the whole equatorial Pacific warmed up and the El Niño conditions formed.

4. Conclusion and discussion

In this work, the evolution of the 2018/19 El Niño was investigated. The 2018/19 El Niño is classified as a CP-I El Niño according to existing classification methods. However, heat budget analysis demonstrated that the development of the 2018/19 El Niño is mainly attributed to subtropical processes, which is the key feature of a CP-II El Niño. This apparent paradox results from the tortuous developing process of the 2018/19 El Niño, since both equatorial and off-equatorial forcings were extensively involved. In early 2018, both the equatorial and subtropical conditions were favorable for the development of an El Niño event. While the favorable equatorial conditions faded and even reversed in boreal summer, the positive Ekman feedback caused by subtropical westerly anomalies kept the western-central Pacific SST increasing. Consequently, the subtropical factor took control of the development process and finally materialized a CP-II El Niño. It is illustrated that forcing factors from the equatorial and subtropical Pacific have the potential to promote an El Niño together, like the widely discussed 2015/16 El Niño (Huo and Xiao, 2016; Palmeiro et al., 2017). Although the influences of equatorial and off-equatorial forcing elements on the development of El Niño events have been discussed in previous studies (Yu et al., 2010; Chen et al., 2018; Yeh et al., 2018), their joint effect is seldom addressed. The findings of this study demonstrate that various driving forces may coexist in a particular El Niño event and play different roles in different stages. This is the reason for the inconsistency between the classification result and the evolution features of the 2018/19 El Niño. Such a hybrid situation is not considered in the existing classification approaches. To improve the classification, a more sophisticated method is needed. Perhaps the components of the CP-II index can be subdivided. Or in a more direct and mechanistic way, the contributions of the zonal and vertical advective feedbacks could be used; an understanding of their combined effect will help us better understand the complexity of ENSO diversity and improve ENSO prediction skill.

The importance of wind anomalies in the northern subtropical Pacific is revealed in this work. Yet the source of these wind anomalies has not been clear. Previous studies have suggested that the North Pacific Oscillation (NPO, Rogers, 1981) and Pacific Meridional mode (PMM, Chiang et al., 2004) in the subtropical North Pacific play an important role in the onset of the CP El Niño (Yu and Kim, 2011; Yeh et al., 2015; Wang et al., 2019b). The westerly anomalies in the subtropical northern Pacific, which are demonstrated to be a crucial forcing for the 2018/19 El Niño in this study, are closely related to both the NPO and PMM. The impacts of the NPO and PMM on the generations of other CP El Niño events will be explored in a follow-up study. Another crucial element that affected the development of the 2018/19 El Niño is the reversal of the central equatorial wind anomalies from westerly to easterly in the boreal summer of 2018. This equatorial forcing element is likely to be a result of the large zonal SST anomaly (SSTA) gradient in the equatorial Pacific, which is associated with positive (negative) SSTA in the western (eastern) Pacific (Fig. S4, January–June). It is also suggested that the mean state of the Pacific (negative phase of the Pacific Decadal Oscillation /Interdecadal Pacific Oscillation) is favorable for the formation of the easterly anomalies in the tropical Pacific (Min et al., 2015; Hu and Fedorov, 2016). The interrelationship between these intraseasonal and decadal stimuli deserve further analysis. In addition, a coupled model will be needed to further quantify the effects of equatorial and off-equatorial forcings.

Acknowledgements. This work is supported by the National Natural Science Foundation of China (Grant Nos. 41925024 and 41876021), Strategic Priority Research Program of Chinese Academy of Sciences (Grant No. XDB42000000), Key Special Project for Introduced Talents Team of Southern Marine Science and Engineering Guangdong Laboratory (Guangzhou) (GML2019ZD0306), Innovation Academy of South China Sea Ecology and Environmental Engineering, Chinese Academy of Sciences (ISEE2021ZD01), and Natural Science Foundation of Shandong Province, China (Grant No. ZR2020QD065).

Electronic supplementary material: Supplementary material is available in the online version of this article at https://doi.org/10.1007/s00376-022-1410-1.

REFERENCES

Ashok, K., S. K. Behera, S. A. Rao, H. Y. Weng, and T. Yamagata, 2007: El Niño Modoki and its possible teleconnection. *J. Geophys. Res.*, **112**(C11), C11007, https://doi.org/10.1029/2006JC003798.

Behringer, D. W., and Y. Xue, 2004: Evaluation of the global ocean data assimilation system at NCEP: The Pacific Ocean. *Eighth Symposium on Integrated Observing and Assimilation Systems for Atmosphere, Oceans, and Land Surface, AMS 84th Annual Meeting*, Washington State Convention and Trade Center, Seattle, Washington, 11–15.

Bjerknes, J., 1969: Atmospheric teleconnections from the equatorial Pacific. *Mon. Wea. Rev.*, **97**(3), 163–172, https://doi.org/10.1175/1520-0493(1969)097<0163:ATFTEP>2.3.CO;2.

Capotondi, A., and Coauthors, 2015: Understanding ENSO diversity. *Bull. Amer. Meteor. Soc.*, **96**, 921–938, https://doi.org/10.1175/BAMS-D-13-00117.1.

Carton, J. A. and B. S. Giese, 2008: A Reanalysis of Ocean Climate

Using Simple Ocean Data Assimilation (SODA). *Mon. Weather Rev.*, **136**, 2999–3017, https://doi.org/10.1175/2007MWR1978.1.

Chen, D. K., and Coauthors, 2015: Strong influence of westerly wind bursts on El Niño diversity. *Nature Geoscience*, **8**(5), 339–345, https://doi.org/10.1038/ngeo2399.

Chen, M. Y., J.-Y. Yu, X. Wang, and W. P. Jiang, 2019: The changing impact mechanisms of a diverse El Niño on the Western Pacific subtropical high. *Geophys. Res. Lett.*, **46**(2), 953–962, https://doi.org/10.1029/2018GL081131.

Chen, M. Y., T.-H. Chang, C.-T. Lee, S.-W. Fang, and J.-Y. Yu, 2021a: A study of climate model responses of the western Pacific subtropical high to El Niño diversity. *Climate Dyn.*, **56**, 581–595, https://doi.org/10.1007/s00382-020-05500-2.

Chen, M. Y., J.-Y. Yu, X. Wang, and S. Chen, 2021b: Distinct onset mechanisms of two subtypes of CP El Niño and their changes in future warming. *Geophys. Res. Lett.*, **48**, e2021GL093707, https://doi.org/10.1029/2021GL093707.

Chen, S. F., B. Yu, W. Chen, and R. G. Wu, 2018: A review of atmosphere-ocean forcings outside the Tropical Pacific on the El Niño-southern oscillation occurrence. *Atmosphere*, **9**, 439, https://doi.org/10.3390/atmos9110439.

Chiang, J. C. H., and D. J. Vimont, 2004: Analogous Pacific and Atlantic meridional modes of tropical atmosphere-ocean variability. *J. Climate*, **17**, 4143–4158, https://doi.org/10.1175/JCLI4953.1.

Compo, G. P., and Coauthors, 2011: The twentieth century reanalysis project. *Quart. J. Roy. Meteor. Soc.*, **137**(654), 1–28, https://doi.org/10.1002/qj.776.

Fang, S.-W., and J.-Y. Yu, 2020: A control of ENSO transition complexity by Tropical Pacific mean SSTs through tropical-subtropical interaction. *Geophys. Res. Lett.*, **47**, e2020GL087933, https://doi.org/10.1029/2020GL087933.

Giese, B. S., and S. Ray, 2011: El Niño variability in simple ocean data assimilation (SODA), 1871–2008. *J. Geophys. Res.*, **116**, C02024, https://doi.org/10.1029/2010JC006695.

Hu, S. N., and A. V. Fedorov, 2016: Exceptionally strong easterly wind burst stalling El Niño of 2014. *Proceedings of the National Academy of Sciences of the United States of America*, **113**(8), 2005–2010, https://doi.org/10.1073/pnas.1514182113.

Huang, B. Y., Y. Xue, D. X. Zhang, A. Kumar, and M. J. McPhaden, 2010: The NCEP GODAS ocean analysis of the tropical pacific mixed layer heat budget on seasonal to interannual time scales. *J. Climate*, **23**(18), 4901–4925, https://doi.org/10.1175/2010JCLI3373.1.

Huang, B. Y., and Coauthors, 2017: Extended reconstructed sea surface temperature, version 5 (ERSSTv5): Upgrades, validations, and intercomparisons. *J. Climate*, **30**(20), 8179–8205, https://doi.org/10.1175/JCLI-D-16-0836.1.

Huo, W.-J., and Z.-N. Xiao, 2016: The impact of solar activity on the 2015/16 El Niño event. *Atmos. Ocean. Sci. Lett.*, **9**(6), 428–435, https://doi.org/10.1080/16742834.2016.1231567.

Kalnay, E., and Coauthors, 1996: The NCEP/NCAR 40-year reanalysis project. *Bull. Amer. Meteor. Soc.*, **77**, 437–472, https://doi.org/10.1175/1520-0477(1996)077<0437:TNYRP>2.0.CO;2.

Kao, H.-Y., and J.-Y. Yu, 2009: Contrasting eastern-pacific and central-pacific types of ENSO. *J. Climate*, **22**(3), 615–632, https://doi.org/10.1175/2008JCLI2309.1.

Kim, J.-W., T.-H. Chang, C.-T. Lee, and J.-Y. Yu, 2021: On the varying responses of East Asian winter monsoon to three types of El Nino: Observations and model hindcasts. *J. Climate*, **34**, 4089–4101, https://doi.org/10.1175/JCLI-D-20-0784.1.

Kug, J.-S., F.-F. Jin, and S.-I. An, 2009: Two types of El Niño events: Cold tongue El Niño and warm pool El Niño. *J. Climate*, **22**(6), 1499–1515, https://doi.org/10.1175/2008JCLI2624.1.

Lai, A. W.-C., M. Herzog, and H.-F. Graf, 2015: Two key parameters for the El Niño continuum: Zonal wind anomalies and Western Pacific subsurface potential temperature. *Climate Dyn.*, **45**(11–12), 3461–3480, https://doi.org/10.1007/s00382-015-2550-0.

Larkin, N. K., and D. E. Harrison, 2005: On the definition of El Niño and associated seasonal average U.S. weather anomalies. *Geophys. Res. Lett.*, **32**(13), L13705, https://doi.org/10.1029/2005GL022738.

Liu, L., G. Yang, X. Zhao, L. Feng, G. Q. Han, Y. Wu, and W. D. Yu, 2017: Why was the Indian Ocean dipole weak in the context of the extreme El Niño in 2015. *J. Climate*, **30**(12), 4755–4761, https://doi.org/10.1175/JCLI-D-16-0281.1.

Liu, Q.-Y., D. X. Wang, X. Wang, Y. Q. Shu, Q. Xie, and J. Chen, 2014: Thermal variations in the South China Sea associated with the eastern and central Pacific El Niño events and their mechanisms. *J. Geophys. Res.*, **119**(12), 8955–8972, https://doi.org/10.1002/2014JC010429.

Liu, Y. Y., Z.-Z. Hu, and R. G. Wu, 2020: Was the extremely wet winter of 2018/2019 in the lower reach of the Yangtze River driven by El Niño-Southern Oscillation. *International Journal of Climatology*, **40**, 6441–6457, https://doi.org/10.1002/joc.6591.

Min, Q. Y., J. Z. Su, R. H. Zhang, and X. Y. Rong, 2015: What hindered the El Niño pattern in 2014. *Geophys. Res. Lett.*, **42**, 6762–6770, https://doi.org/10.1002/2015GL064899.

Palmeiro, F. M., M. Iza, D. Barriopedro, N. Calvo, and R. García-Herrera, 2017: The complex behavior of El Niño winter 2015–2016. *Geophys. Res. Lett.*, **44**(6), 2902–2910, https://doi.org/10.1002/2017GL072920.

Rogers, J. C. 1981: The North Pacific oscillation. *International Journal of Climatology*, **1**(1), 39–57, https://doi.org/10.1002/joc.3370010106.

Schneider, U., A. Becker, P. Finger, A. Meyer-Christoffer, B. Rudolf, and M. Ziese, 2011: GPCC full data reanalysis version 6.0 at 1.0: Monthly land-surface precipitation from rain-gauges built on GTS-based and historic data, https://doi.org/10.5676/DWD_GPCC/FD_M_V6_100.

Schneider, U., A. Becker, P. Finger, A. Meyer-Christoffer, B. Rudolf, and M. Ziese, 2016: GPCC full data reanalysis version 7.0: Monthly land-surface precipitation from rain gauges built on GTS based and historic data, https://doi.org/10.5065/D6000072.

Tan, W., X. Wang, W. Q. Wang, C. Z. Wang, and J. C. Zuo, 2016: Different responses of sea surface temperature in the South China sea to various El Niño events during boreal autumn. *J. Climate*, **29**(3), 1127–1142, https://doi.org/10.1175/JCLI-D-15-0338.1.

Vimont, D. J., D. S. Battisti, and A. C. Hirst, 2001: Footprinting: A seasonal connection between the tropics and mid-latitudes. *Geophys. Res. Lett.*, **28**, 3923–3926, https://doi.org/10.1029/2001GL013435.

Wang, C. Z., and X. Wang, 2013: Classifying El Niño Modoki I and II by different impacts on rainfall in southern China and typhoon tracks. *J. Climate*, **26**(4), 1322–1338, https://doi.

org/10.1175/JCLI-D-12-00107.1.

Wang, W., F. Xin, X. Pan, Y. Zhang, and T. Li, 2020a: Seasonal and sub-seasonal circulation anomalies associated with persistent rainy days in 2018/2019 winter in Shanghai, China. *Journal of Meteorological Research*, **34**(2), 304–314, https://doi.org/10.1007/s13351-020-9163-1.

Wang, X., and C. Z. Wang, 2014: Different impacts of various El Niño events on the Indian Ocean Dipole. *Climate Dyn.*, **42**(3-4), 991–1005, https://doi.org/10.1007/s00382-013-1711-2.

Wang, X., W. Tan, and C. Z. Wang, 2018: A new index for identifying different types of El Niño Modoki events. *Climate Dyn.*, **50**(7), 2753–2765, https://doi.org/10.1007/s00382-017-3769-8.

Wang, X., M. Y. Chen, C. Z. Wang, S.-W. Yeh, and W. Tan, 2019b: Evaluation of performance of CMIP5 models in simulating the North Pacific Oscillation and El Niño Modoki. *Climate Dyn.*, **52**, 1383–1394, https://doi.org/10.1007/s00382-018-4196-1.

Wang, X., C. Y. Guan, R. X. Huang, W. Tan, and L. Wang, 2019c: The roles of tropical and subtropical wind stress anomalies in the El Niño Modoki onset. *Climate Dyn.*, **52**, 6585–6597, https://doi.org/10.1007/s00382-018-4534-3.

Wang, X., B. Tong, D. X. Wang, and L. Yang, 2020b: Variations of the North Equatorial current bifurcation and the SSH in the Western Pacific associated with El Niño flavors. *J. Geophys. Res.*, **125**, e2019JC015733, https://doi.org/10.1029/2019JC015733.

Xie, S.-P., and S. G. H. Philander, 1994: A coupled ocean-atmosphere model of relevance to the ITCZ in the eastern Pacific. *Tellus A: Dynamic Meteorology and Oceanography*, **46**(4), 340–350, https://doi.org/10.3402/tellusa.v46i4.15484.

Yeh, S.-W., X. Wang, C. Z. Wang, and B. Dewitte, 2015: On the relationship between the north Pacific climate variability and the central Pacific El Niño. *J. Climate*, **28**, 663–677, https://doi.org/10.1175/JCLI-D-14-00137.1.

Yeh, S.-W., D.-W. Yi, M.-K. Sung, and Y. H. Kim, 2018: An eastward shift of the North Pacific oscillation after the mid-1990s and its relationship with ENSO. *Geophys. Res. Lett.*, **45**(13), 6654–6660, https://doi.org/10.1029/2018GL078671.

Yu, J.-Y., and H.-Y. Kao, 2007: Decadal changes of ENSO persistence barrier in SST and ocean heat content indices: 1958–2001. *J. Geophys. Res.*, **112**(13), D13106, https://doi.org/10.1029/2006JD007654.

Yu, J.-Y., and S. T. Kim, 2011: Relationships between extratropical sea level pressure variations and the Central Pacific and Eastern Pacific types of ENSO. *J. Climate*, **24**, 708–720, https://doi.org/10.1175/2010JCLI3688.1.

Yu, J.-Y., and S.-W. Fang, 2018: The distinct contributions of the seasonal footprinting and charged-discharged mechanisms to ENSO complexity. *Geophys. Res. Lett.*, **45**, 6611–6618, https://doi.org/10.1029/2018GL077664.

Yu, J.-Y., H.-Y. Kao, and T. Lee, 2010: Subtropics-related interannual sea surface temperature variability in the central equatorial pacific. *J. Climate*, **23**(11), 2869–2884, https://doi.org/10.1175/2010JCLI3171.1.

Yu, J.-Y., X. Wang, S. Yang, H. Paek, and M. Y. Chen, 2017: The changing El Niño-southern oscillation and associated climate extremes. *Climate Extremes*: *Patterns and Mechanisms*, Wang et al., Eds., American Geophysical Union, https://doi.org/10.1002/9781119068020.ch1.